

# Constraining the Anisotropic Expansion of Universe

Rong-Gen Cai<sup>1,\*</sup> Yin-Zhe Ma<sup>2,3,†</sup> Bo Tang<sup>1,‡</sup> and Zhong-Liang Tuo<sup>1§</sup>

<sup>1</sup> *Key Laboratory of Frontiers in Theoretical Physics,*

*Institute of Theoretical Physics, Chinese Academy of Sciences,*

*P.O. Box 2735, Beijing 100190, China.*

<sup>2</sup> *Department of Physics and Astronomy,*

*University of British Columbia, Vancouver, V6T 1Z1, BC Canada.*

<sup>3</sup> *Canadian Institute for Theoretical Astrophysics,*

*Toronto, M5S 3H8, Ontario, Canada.*

(Dated: October 22, 2022)

## Abstract

We study the possibly existing anisotropy in the accelerating expansion Universe with the Union2 Type Ia supernovae data and Gamma-ray burst data. We construct a direction-dependent dark energy model and constrain the anisotropy direction and strength of modulation. We find that the maximum anisotropic deviation direction is  $(l, b) = (126^\circ, 13^\circ)$  (or equivalently  $(l, b) = (306^\circ, -13^\circ)$ ), and the anisotropy level is  $g_0 = 0.030_{-0.010}^{+0.030}$  (obtained using Union2 data, at  $1\sigma$  confidence level). Our results do not show strong evidence for the anisotropic dark energy model. We also discuss potential methods that may distinguish the peculiar velocity field from the anisotropic dark energy model.

---

\*Electronic address: cairg@itp.ac.cn

†Electronic address: mayinzhe@phas.ubc.ca

‡Electronic address: tangbo.bit@163.com

§Electronic address: tuoql@itp.ac.cn

## 1. INTRODUCTION

The cosmological principle has played an important role in modern cosmology [1]. It tells us that our universe is homogeneous and isotropic on large cosmic scale, which is consistent with currently observational data sets such as the cosmic microwave background (CMB) radiation data from the Wilkinson Microwave Anisotropy Probe (WMAP) [2–4]. Up to now, current astronomical observations are still in good agreement with  $\Lambda CDM$  model generally [5].

Despite the fact that the concordance cosmological model ( $\Lambda CDM$  model) is confirmed by many observational data, the model is also challenged by some observations [6, 7] (see [8] and references therein for more details). So, it is necessary to revisit the assumption of cosmological principle. As more Type Ia supernovae data [9, 10] and high-redshift Gamma-ray burst (GRB) data are released [11, 12], one can use the supernovae data and the GRB data to detect the anisotropic direction of cosmic expansion.

Theoretically, a variety of cosmological models may give rise to cosmic anisotropy. For example, peculiar velocities may generate dipole-like anisotropies, and lead observers to find that the acceleration is maximized in one direction but minimized in the opposite [13]. A vector field may cause cosmic anisotropy and lead to a direction-dependent dark energy equation of state [14]. Using Union2, Ref. [15] derived the angular covariance function of the standard candle magnitude fluctuations, but they did not find any angular scales where the covariance function deviates from 0 in a statistically significant manner. By using 288 SNIa [16], Davis *et al.* [17] studied the effects of peculiar velocities, taking into consideration of our own peculiar motion, supernova’s motion and coherent bulk motion, and they found that it would cause a systematic shift  $\Delta w = 0.02$  in the equation of state of dark energy if we neglected coherent velocities. Gupta *et al.* [18] introduced a statistic based on the extreme value theory and applied it to the gold data set of SNIa, and they showed that the data is consistent with isotropy and Gaussianity. In contrast to these “null-results”, Ref. [19] constructed a “residual” statistic to search for the preferred direction in different slices of past light-cone, and they found that at low redshift ( $z < 0.5$ ) an isotropic model was not consistent with the SNIa data even at  $2\text{-}3\sigma$ . Ref. [20] found that anisotropy was permitted both in the geometry of the universe and in the dark energy equation of state, if we worked in the frame work of an anisotropic Bianchi type I cosmological model and the presence of an

anisotropic dark energy equation of state. Additionally, Refs. [21–23] used the hemisphere comparison method to fit the  $\Lambda CDM$  model (and  $wCDM$  model) to the supernovae data, and detected a preferred axis at statistically significant level. These results are consistent with many other observations, such as the CMB dipole [24], large scale alignment in the QSO optical polarization data [25] and large scale velocity flows [26].

Ref. [22] obtained the average direction of the preferred axes as  $(l, b) = (278^\circ \pm 26^\circ, 45^\circ \pm 27^\circ)$ . Further analysis was made by [27], they used different low-redshift ( $z < 0.2$ ) SNIa samples and employed the the Hubble parameter to quantify the anisotropy level, and the results showed that all the SNIa samples indicated an anisotropic direction at 95% confidence level.

In this paper we study the plausible anisotropy in the accelerated expanding Universe with the Union2 data. We construct an anisotropic dark energy model and aim to detect the maximum anisotropy direction that deviates from the isotropic dark energy model described by  $\Lambda CDM$  model. Furthermore, we consider the impact of redshift on the direction by using the redshift tomography method, with the high-redshift Gamma-ray burst data as a complement. Finally, we check two other models as the description of the isotropic background. One is the  $wCDM$  model, the other is a dynamical dark energy model represented by the  $CPL$  parametrization [28]. We exam that if our results are dependent on the isotropic background.

The paper is organized as follows. In the next section we give a general introduction to the anisotropic dark energy model, which is based on the isotropic background described by the  $\Lambda CDM$  model, and the  $\chi^2$  statistics of the model with observational data. In Sec. 3, we give the numerical results on the maximum anisotropy directions from the SNIa data and high-redshift GRB data with different slices of redshift. We also give the result for the  $wCDM$  and  $CPL$  model. Our conclusions are presented in the last section.

## 2. ANISOTROPIC DARK ENERGY MODEL

If dark energy has anisotropic repulsive force, it will directly affect the expansion rate of the universe, leading to the anisotropic luminosity distance. This effect should be observable by the luminosity of SNIa. In this paper, we use the Union2 dataset [9], which contains 557 type Ia SNIa data covering the redshift range  $z = [0.015, 1.4]$ .

We try to quantify the deviation from the isotropic background as dipole modulation. By using the luminosity distance we define the deviation from isotropic expansion as

$$\frac{d_L(\vec{z}) - d_L^0(z)}{d_L^0(z)} = g(z)(\hat{z} \cdot \hat{n}). \quad (2.1)$$

where, the true luminosity distance of the supernova is  $d_L(\vec{z})$ , and in an isotropic background, the luminosity distance is  $d_L^0(z)$ .  $g(z)(\hat{z} \cdot \hat{n})$  is the modulation part of the luminosity distance, which makes the real luminosity function anisotropic. Note that the modulation could be any power-law form of  $(\hat{z} \cdot \hat{n})$ , such as  $(\hat{z} \cdot \hat{n})^s$ , where  $s$  is a constant, but we focus on the dipole modulation here ( $s = 1$ ). In principle, one can use this model to discuss quadrupole modulation ( $s = 2$ ), octupole modulation ( $s = 4$ ) and higher moments ( $s > 4$ ).  $\hat{z}$  is the unit direction vector of the supernova, which can be expressed by using the Galactic coordinate system.  $\hat{n}$  is the direction of dark energy dipole, which is the maximal expanding direction,

$$\hat{n} = (\cos \phi \sin \theta, \sin \phi \sin \theta, \cos \theta) \quad (2.2)$$

where  $\theta \in [0, \pi]$  and  $\phi \in [0, 2\pi]$ . For instance, we can parameterize  $g(z)$  with linear function of  $Z$  as

$$g(z) = g_0 + g_1 z. \quad (2.3)$$

where  $g_0$  and  $g_1$  are two constants, representing the strength of modulation and the time evolution of modulation, respectively. Of course, the simplest case is where  $g_1 = 0$ , which corresponds to the case where the direction-dependent modulation is constant over all redshifts.

In a spatially flat isotropic cosmological background, the luminosity distance can be expressed as

$$d_L^0(z) = (1 + z) \int_0^z \frac{H_0}{H(z')} dz'. \quad (2.4)$$

where  $H_0$  is the current Hubble parameter. Accordingly, the theoretical distance modulus  $\mu_{th}$  is defined as

$$\mu_{th}(z) = 5 \log_{10} d_L(z) + \mu_0, \quad \mu_0 = 42.384 - 5 \log_{10} h,$$

where,  $H_0 = 100h \text{ km} \cdot \text{s}^{-1} \cdot \text{Mpc}^{-1}$ .

Since  $\Lambda CDM$  model is consistent with current astronomical observations, it is reasonable to take  $\Lambda CDM$  model as the isotropic cosmological background, in which the Hubble

parameter can be expressed as

$$H^2(z) = H_0^2[\Omega_{m0}(1+z)^3 + (1-\Omega_{m0})]. \quad (2.5)$$

where  $\Omega_{m0}$  is the current value of the energy density fraction of dark matter. While in the case of  $wCDM$  model, the equation of state of dark energy is parametrized by a constant  $w$ ,  $w = p/\rho$ , therefore we have

$$H^2(z) = H_0^2[\Omega_{m0}(1+z)^3 + (1-\Omega_{m0})(1+z)^{3+3w}]. \quad (2.6)$$

And if the background is described by the  $CPL$  parametrization, the equation of state of dark energy is  $w = w_0 + w_1 \frac{z}{1+z}$ . Accordingly one obtains

$$H(z) = H_0^2[\Omega_{m0}(1+z)^3 + (1-\Omega_{m0})(1+z)^{3(1+w_0+w_1)} \exp\left(-\frac{3w_1 z}{1+z}\right)]. \quad (2.7)$$

We employ the Union2 dataset to constrain the anisotropic dark energy model. The directions to the SNIa we use here are given in Ref. [15], and are described in the equatorial coordinates (right ascension and declination). In order to make comparisons with other results, we convert these coordinates to the galactic coordinates  $(l, b)$  [29].

Let us suppose the experiment error between each measurement is completely independent, so the covariance matrix can be simplified as the diagonal component, and the  $\chi_{sn}^2$  can be written as

$$\chi_{sn}^2 = \sum_{i=1}^{557} \frac{[\mu^{obs}(z_i) - \mu^{th}(z_i)]^2}{\sigma^2(z_i)}.$$

where,  $\mu^{obs}(z_i)$  is the measured distance modulus from the Union2 data, and  $\mu^{th}(z_i)$  is the direction-depedent theoretical distance modulus.

We can eliminate the nuisance parameter  $\mu_0$  by expanding  $\chi_{sn}^2$  with respect to  $\mu_0$  [30]:

$$\chi_{sn}^2 = A + 2B\mu_0 + C\mu_0^2, \quad (2.8)$$

where

$$\begin{aligned} A &= \sum_i \frac{[\mu_{th}(z_i; \mu_0 = 0) - \mu_{obs}(z_i)]^2}{\sigma^2(z_i)}, \\ B &= \sum_i \frac{\mu_{th}(z_i; \mu_0 = 0) - \mu_{obs}(z_i)}{\sigma^2(z_i)}, \\ C &= \sum_i \frac{1}{\sigma^2(z_i)}. \end{aligned}$$

The  $\chi_{sn}^2$  has a minimum as

$$\tilde{\chi}_{SN}^2 = A - B^2/C , \quad (2.9)$$

which is independent of  $\mu_0$ . This technique is equivalent to performing a uniform marginalization over  $\mu_0$  [30]. We will adopt  $\tilde{\chi}_{sn}^2$  as the goodness of fitting instead of  $\chi_{sn}^2$ .

Combining with Eq. (2.4) and substituting each anisotropic model in the  $\tilde{\chi}_{sn}^2$ , one can easily calculate the likelihood function of each parameter by performing the Markov Chain Monte Carlo analysis. The parameters need to be constrained are  $(g_0, g_1, \theta, \phi)$ , where  $(\theta, \phi)$  is the direction of modulation. We then convert  $(\theta, \phi)$  into galactic coordinate  $(l, b)$ .

### 3. REDSHIFT TOMOGRAPHY

Following the procedure introduced in Sec.2, one can obtain the best-fitting values and errors of parameters by performing the Monte Carlo Markov Chain analysis in the multidimensional parameter space. During the procedure, we use the best-fitting values obtained by WMAP group to calculate  $d_L^0(z)$  in the isotropic background. We choose  $\Omega_{m0} = 0.274$  for  $\Lambda CDM$  model,  $\Omega_{m0} = 0.274$ ,  $w = -1.037$  for  $wCDM$  model, and  $\Omega_{m0} = 0.274$ ,  $w_0 = -1.17$ ,  $w_1 = 0.35$  for  $CPL$  parametrization, which are obtained using  $WMAP + eCMB + BAO + H_0 + SNe$  datasets [4].

In order to explore the possible redshift dependence of the anisotropy, we implement a redshift tomography analysis, taking the same procedure as before for the following redshift slices: 0-0.2, 0-0.4, 0-0.6, 0-0.8, 0-1.0, 0-1.2, 0-1.4. Our results for  $\Lambda CDM$  model are summarized in Table 1. We also use the GRB data to explore the high-redshift behavior, which can extend our detection to  $z = 6.6$ . In this paper, we have compiled 67 GRB data in total as shown in Table 6. These samples are selected from [11, 12] and we add in the position of each data point (for more details, please visit the website [35]). The last row of Table 1 shows the fitting result by combining Union2 Type Ia supernovae with the GRB samples.

The redshift tomography analysis here shows that the preferred axes at different redshifts are all located in a relatively small redion of the Galactic Hemisphere ( $\sim (l, b) = (126^\circ, 13^\circ)$  for Union2 data). Note that the meaning of this best-fitting direction is the same as  $(l, b) = (306^\circ, -13^\circ)$ , because both directions are located on the same axis, and both are directions of maximum deviation from the  $\Lambda CDM$  model. The best-fitting direction is consistent with

redshift range	$l$ [degree]	$b$ [degree]	$g_0$	$g_1$
0 – 0.2	$134^{-23-91}_{+13+212}$	$4^{-7-59}_{+30+41}$	$0.045^{-0.044-0.045}_{+0.026+0.063}$	$-0.289^{-0.713-1.648}_{+0.410+1.013}$
0 – 0.4	$125^{-18-60}_{+17+255}$	$8^{-7-88}_{+24+35}$	$0.036^{-0.028-0.036}_{+0.016+0.025}$	$-0.093^{-0.107-0.251}_{+0.163+0.354}$
0 – 0.6	$121^{-18-81}_{+17+255}$	$10^{-7-88}_{+24+35}$	$0.033^{-0.033-0.033}_{+0.018+0.026}$	$-0.077^{-0.039-0.075}_{+0.099+0.163}$
0 – 0.8	$128^{-22-88}_{+17+265}$	$15^{-25-100}_{+19+63}$	$0.030^{-0.030-0.030}_{+0.013+0.024}$	$-0.022^{-0.071-0.114}_{+0.064+0.185}$
0 – 1.0	$123^{-27-89}_{+20+269}$	$14^{-22-79}_{+20+55}$	$0.031^{-0.031-0.031}_{+0.012+0.024}$	$-0.040^{-0.050-0.097}_{+0.056+0.092}$
0 – 1.2	$125^{-33-90}_{+19+265}$	$12^{-29-71}_{+20+43}$	$0.032^{-0.032-0.032}_{+0.013+0.032}$	$-0.042^{-0.047-0.086}_{+0.050+0.082}$
0 – 1.4	$126^{-26-92}_{+17+266}$	$13^{-25-82}_{+19+39}$	$0.030^{-0.030-0.030}_{+0.010+0.021}$	$-0.031^{-0.039-0.075}_{+0.042+0.069}$
0 – 6.6	$129^{-23-96}_{+16+293}$	$16^{-10-89}_{+17+54}$	$0.028^{-0.028-0.028}_{+0.013+0.021}$	$-0.006^{-0.034-0.055}_{+0.025+0.052}$

Table 1: Constraints of the directions and amplitude of maximum anisotropy for different redshift bins of the Union2 data and GRB data. The error-bars quoted are  $1\sigma$  and  $2\sigma$  errors.

the result in Ref. [31] at  $1\sigma$  confidence level. We also re-examined the dark energy dipole by using the Union2 data with the same method proposed in Ref. [31], showing that the dark energy dipole is indeed aligned with the corresponding fine structure constant cosmic dipole, where the dark energy dipole direction is ( $l = 309.4^\circ \pm 18.0^\circ$ ,  $b = -15.1^\circ \pm 11.5^\circ$ ) and the fine structure dipole direction is ( $l = 320.5^\circ \pm 11.8^\circ$ ,  $b = -11.7^\circ \pm 7.5^\circ$ ).

We plot the likelihood of the parameters ( $g_0$ ,  $g_1$ ,  $l$ ,  $b$ ) in Fig 1. It is obvious from Eq (2.1) that there are two maximum anisotropic directions, which are settled on the same axis, accordingly  $g(z)$  can be positive or negative. Note that in our calculations, we have set  $g_0 > 0$ , but the maximum anisotropic axis does not change if we set  $g_0 < 0$ .

Furthermore, we constrain the redshift dependence of the anisotropy by using SNIa data located only in different redshift bins: 0-0.2, 0.2-0.4, 0.4-0.6, 0.6-0.8, 0.8-1.0, thus to avoid influences from other bins. Accordingly, we obtain 220, 124, 102, 50 and 41 data points in different redshift bins respectively. Our results for  $\Lambda CDM$  model are summarized in Table 2. Figure 2 shows the best-fitting  $g(z)$  with  $1\sigma$  error at different redshifts. It is clear that the anisotropy level  $g(z)$  is close to 0, which means that the  $\Lambda CDM$  model is still consistent with the Union2 data very well. The error increases as redshift increases, and we can not

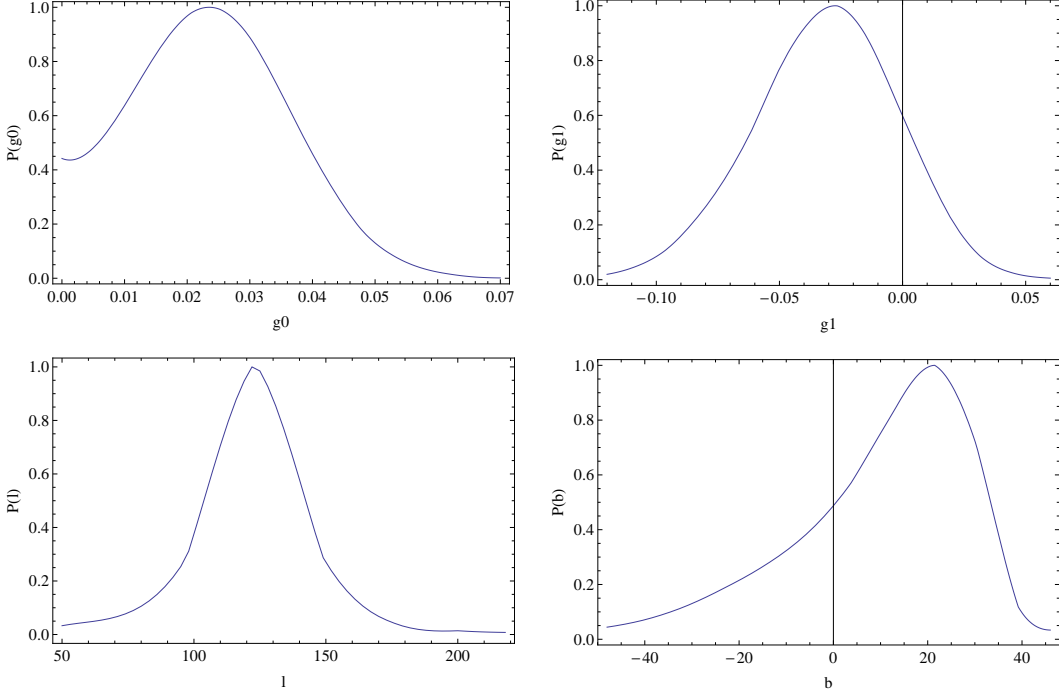


Fig. 1: Likelihoods for parameters  $(g_0, g_1, l, b)$  using the full Union2 data, with the best-fitting parameters  $(g_0 = 0.030, g_1 = -0.031, l = 126^\circ, b = 13^\circ)$ .

exclude the case  $g(z) = 0$  even at 68.3% confidence level. Note that the anisotropic direction changes as redshift bin changes, but these directions are consistent with each other at 68.3% confidence level.

By considering the case of  $g(z) = g_0$  and using the full Union2 data, we obtain Table 3, which shows that the maximum deviation from the  $\Lambda CDM$  model is 0.024, and the maximum anisotropy direction is similar to the results in Table 1, but we still can not exclude the case  $g_0 = 0$  at  $1\sigma$  confidence level.

We also consider the  $wCDM$  and the  $CPL$  parameterized dark energy models as the isotropic background. We use  $w$  and  $(w_0, w_1)$  as the isotropic background dark energy parameters and fit our anisotropic parameters, respectively, and the results are summarized in Table 4. The results of constraints on  $(l, b, g_0, g_1)$  are not much different from the case of the  $\Lambda CDM$  model. This means that the best-fitting value of the maximum deviation direction from the isotropic background is not sensitive to the details of isotropic dark energy models.

redshift range	$l$ [degree]	$b$ [degree]	$g_0$	$g_1$
0 – 0.2	$134^{-23-91}_{+13+212}$	$4^{-7-59}_{+30+41}$	$0.045^{-0.044-0.045}_{+0.026+0.063}$	$-0.289^{-0.713-1.648}_{+0.410+1.013}$
0.2 – 0.4	$253^{-167-220}_{+107+138}$	$-49^{-4-34}_{+89+133}$	$0.086^{-0.086-0.086}_{+0.287+0.552}$	$-0.309^{-1.073-1.670}_{+0.439+0.616}$
0.4 – 0.6	$334^{-279-301}_{+56+59}$	$-18^{-24-58}_{+53+108}$	$0.487^{-0.487-0.487}_{+0.412+0.511}$	$-0.077^{-0.039-0.075}_{+0.099+0.163}$
0.6 – 0.8	$149^{-115-116}_{+241+244}$	$63^{-106-140}_{+10+25}$	$0.163^{-0.163-0.163}_{+0.787+0.833}$	$-0.191^{-1.138-1.257}_{+0.270+0.330}$
0.8 – 1.0	$146^{-96-113}_{+233+246}$	$-6^{-33-68}_{+46+90}$	$0.997^{-0.996-0.997}_{+0.003+0.003}$	$-1.111^{-0.293-0.293}_{+1.355+1.355}$

Table 2: Constraints on direction and strength of modulation for several redshift bins of the Union2 data fitting with the  $\Lambda CDM$  model, together with the  $1\sigma$  and  $2\sigma$  errors of parameters ( $l$ ,  $b$ ,  $g_0$ ,  $g_1$ ).

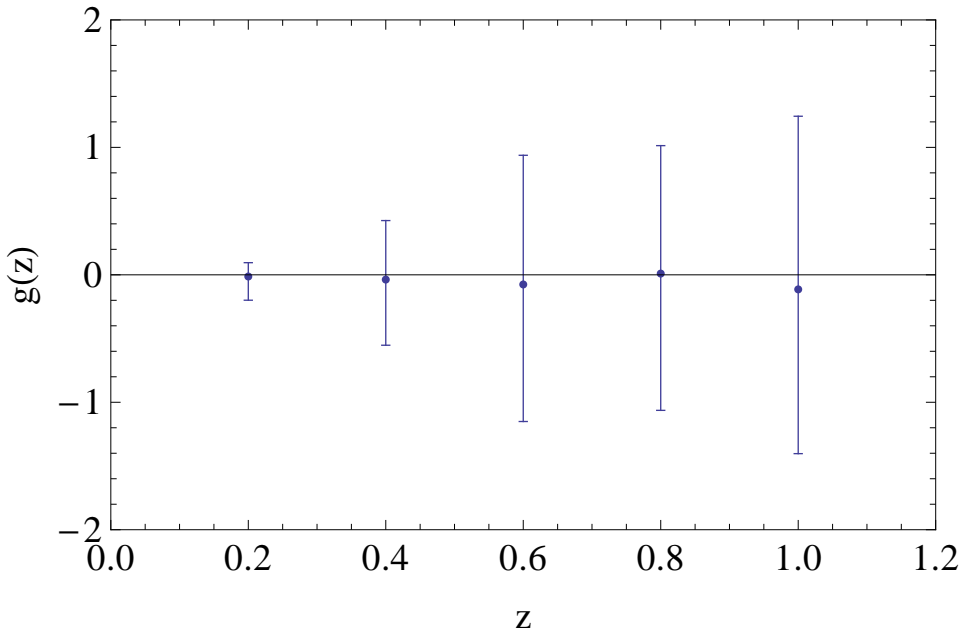


Fig. 2: Best-fitting  $g(z)$  with  $1\sigma$  error at different redshift.

$l$ [degree]	$b$ [degree]	$g_0$
$128^{-23-94}_{+22+264}$	$16^{-14-97}_{+21+64}$	$0.024^{-0.024-0.024}_{+0.008+0.021}$

Table 3: Constraints on direction and strength of modulation for the full Union2 data fitting with the  $\Lambda CDM$  model, together with the  $1\sigma$  and  $2\sigma$  errors of parameters ( $l$ ,  $b$ ,  $g_0$ ).

In the end, we make Bayesian statistical comparison between the isotropic dark energy models and the anisotropic dark energy models, in order to see which model is more favored

Models	$l$ [degree]	$b$ [degree]	$g_0$	$g_1$
$wCDM$	$128_{+17+256}^{-28-88}$	$14_{+17+39}^{-30-74}$	$0.034_{+0.013+0.026}^{-0.033-0.034}$	$-0.045_{+0.049+0.090}^{-0.056-0.093}$
$CPL$	$127_{+17+230}^{-21-80}$	$15_{+17+61}^{-32-77}$	$0.035_{+0.015+0.027}^{-0.035-0.035}$	$-0.049_{+0.049+0.102}^{-0.046-0.347}$

Table 4: Directions of maximum anisotropy fitting with the  $wCDM$  model and  $CPL$  model, together with the  $1\sigma$  and  $2\sigma$  errors of parameters ( $l$ ,  $b$ ,  $g_0$ ,  $g_1$ ).

by observational data. The Bayesian Evidence  $E$  provides us with a good metric to quantify the level of consistency between each model and observational data [33],

$$BE = \int \mathcal{L}(D|\theta, H)p(\theta|H)d\theta.$$

The ratio of Evidences between the two models  $B_{AB} \equiv E(A)/E(B)$ , also known as the Bayes factor, measures the goodness of fit of the models. In the following, we calculate the Bayesian Evidence ratio of the anisotropic model ( $A$ ) and the isotropic model ( $B$ ) by assuming the uniform prior for every parameter. According to the Jeffreys grades, the result is summarized as follows (see Table 5).

Models	Parameters	Bayes factor	Comparison
$\Lambda CDM$	$\Omega_{m0}$	-0.35	Weak
$wCDM$	$\Omega_{m0}, w$	1.08	Significant
$CPL$	$\Omega_{m0}, w_0, w_1$	3.17	Strong to very strong

Table 5: Comparison result using the Bayes factor for anisotropic and isotropic dark energy models.

- (1) If the background is described by the  $\Lambda CDM$  model, the parameters for isotropic and anisotropic models are  $(\Omega_{m0})$  and  $(l, b, g_0, g_1)$ , respectively. The Bayes factor is -0.35, which means that there is “weak” evidence that the  $\Lambda CDM$  model is better than the anisotropic model.
- (2) If the background is described by the  $wCDM$  model, the parameters for isotropic and anisotropic models are  $(\Omega_{m0}, w)$  and  $(l, b, g_0, g_1)$ , respectively. The Bayes factor is 1.08, which means that there is “significant” evidence that the anisotropic model is better than the  $wCDM$  model.

(3) If the background is described by the *CPL* parametrization, the parameters for isotropic and anisotropic models are  $(\Omega_{m0}, w_0, w_1)$  and  $(l, b, g_0, g_1)$ , respectively. The Bayes factor is 3.17, which means that there is “strong to very strong” evidence that the anisotropic dark energy model is better than the *CPL* parametrization.

### A. Distinguish Anisotropic Dark Energy With Peculiar Velocity Field Model

In this paper, we consider the model of anisotropic dark energy, which may potentially be degenerated with the peculiar velocity field model in an isotropic background. For example, the best-fitting bulk flow direction found in Ref. [34] is quite close to the direction  $(l, b) = (306^\circ, -13^\circ)$ . . This is because, the peculiar motion of galaxies or supernovae can also produce a direction-dependent luminosity distance, which may indicate some preferred direction. With the current data at low redshift, we are not able to distinguish them, but we propose the following method which is useful for doing this in advance of new data.

First, if the anisotropy is caused by the peculiar velocity, the anisotropic direction should be randomly distributed on different cosmic scales, because peculiar velocity is driven by emergent of large scale structure, but if the anisotropy is caused by the dark energy dipole, the anisotropic direction should be a constant on all cosmic scale, due to the non-local effect of dark energy. So redshift tomography method may tell the differences between the two models if high-z SNIa data are available.

Second, peculiar velocity is a local effect and should be zero if averaged on the whole cosmic scale [32]. But the dark energy dipole should not change with the redshift. So by average the galaxy luminosity over a large volume, one can distinguish where the direction-dependence of luminosity is due to peculiar velocity or dark energy dipole.

In addition, the Integrated Sachs-Wolfe effect (ISW) can be used to detect the dark energy dipole, because if the accelerating expansion is anisotropic, the photons that travel from different distances in different directions are potentially observable. On the other hand, peculiar motion of galaxies can only re-scatter the CMB photons and produces secondary anisotropic effect, which acquires its maximum at galaxy and cluster scales.

## 4. CONCLUSIONS

There is a tentative evidence that the anisotropic direction on the cosmic expansion exists. If such a cosmological preferred axis indeed exists, one has to consider an anisotropic expanding Universe, instead of the isotropic cosmological model.

In this paper, we investigated the plausible anisotropy in the accelerating expansion Universe with the Union2 data and high-z GRB data. We construct an anisotropic dark energy model, where we quantify the strength of modulation as function  $g(z) = g_0 + g_1 z$  and direction of maximum expansion as  $(l, b)$ . We found that the maximum anisotropic deviation direction is  $(l, b) = (126^\circ, 13^\circ)$  (or equivalently  $(l, b) = (306^\circ, -13^\circ)$ ), and the maximum anisotropy level is described by the parameters  $g_0 = 0.030_{+0.010}^{-0.030}$ ,  $g_1 = -0.031_{+0.042}^{-0.039}$  (obtained using Union2 data, at  $1\sigma$  confidence level). Furthermore, we used the redshift tomography method and found that the anisotropic direction depends on the redshift. However, it is clear that the anisotropy strength  $g(z)$  is close to 0 within  $1\sigma$  confidence level, which indicates that there is no strong evidence against isotropic  $\Lambda CDM$  model.

If the modulation is constant over all redshift, by using the full Union2 data, we found that the maximum deviation from the  $\Lambda CDM$  universe is  $0.024_{+0.008}^{-0.024}$ , and the maximum anisotropy direction is similar to the former results, but we still can not exclude the case  $g_0 = 0$  at  $1\sigma$  confidence level.

We also discussed the cases where the dark energy equation of state is described by a constant  $w$  and  $w(z) = w_0 + w_1 \frac{z}{1+z}$ , respectively, but the results show a similar anisotropic direction. This indicates that the best-fitting value of the maximum deviation direction from the isotropic background is not sensitive to the isotropic dark energy models.

Finally, by using the Bayesian Evidence, we found that the anisotropic dark energy model does not show great statistical evidence better than isotropic  $wCDM$  model, except that there is a slightly greater evidence of anisotropic dark energy than CPL isotropic dark energy model.

### Acknowledgments

This work was supported in part by the National Natural Science Foundation of China (No.10821504, No.10975168 and No.11035008), and in part by the Ministry of Science and

Technology of China under Grant No. 2010CB833004.

This publication was made possible through the support of a grant from the John Templeton Foundation and National Astronomical Observatories of Chinese Academy of Sciences. The opinions expressed in this publication are those of the authors do not necessarily reflect the views of the John Templeton Foundation or National Astronomical Observatories of Chinese Academy of Sciences. The funds from John Templeton Foundation were awarded in a grant to The University of Chicago which also managed the program in conjunction with National Astronomical Observatories, Chinese Academy of Sciences.

---

- [1] S. Weinberg, *Cosmology* (Oxford University Press, New York, New York, 2008).
- [2] E. Komatsu *et al.* [WMAP Collaboration], *Astrophys. J. Suppl.* **192**, 18 (2011) [arXiv:1001.4538 [astro-ph.CO]].
- [3] C. L. Bennett, R. S. Hill, G. Hinshaw, D. Larson, K. M. Smith, J. Dunkley, B. Gold and M. Halpern *et al.*, *Astrophys. J. Suppl.* **192**, 17 (2011) [arXiv:1001.4758 [astro-ph.CO]].
- [4] G. Hinshaw, D. Larson, E. Komatsu, D. N. Spergel, C. L. Bennett, J. Dunkley, M. R. Nolta and M. Halpern *et al.*, arXiv:1212.5226 [astro-ph.CO].
- [5] S. Nesseris and L. Perivolaropoulos, *Phys. Rev. D* **77**, 023504 (2008) [arXiv:0710.1092 [astro-ph]].
- [6] L. Perivolaropoulos, [arXiv:0811.4684 [astro-ph]];  
R. -J. Yang, S. N. Zhang, *Mon. Not. Roy. Astron. Soc.* **407**, 1835-1841 (2010). [arXiv:0905.2683 [astro-ph.CO]]. P. Naselsky, W. Zhao, J. Kim and S. Chen, *Astrophys. J.* **749**, 31 (2012) [arXiv:1108.4376 [astro-ph.CO]].
- [7] A. Mariano and L. Perivolaropoulos, arXiv:1211.5915 [astro-ph.CO].
- [8] L. Perivolaropoulos, arXiv:1104.0539 [astro-ph.CO].
- [9] R. Amanullah *et al.*, *Astrophys. J.* **716**, 712 (2010) [arXiv:1004.1711 [astro-ph.CO]].
- [10] N. Suzuki *et al.*, arXiv:1105.3470 [astro-ph.CO].
- [11] H. Wei, *JCAP* **1008**, 020 (2010) [arXiv:1004.4951 [astro-ph.CO]].
- [12] N. Liang, W. K. Xiao, Y. Liu and S. N. Zhang, arXiv:0802.4262 [astro-ph].
- [13] C. G. Tsagas, arXiv:1107.4045 [astro-ph.CO]; C. G. Tsagas, *Mon. Not. Roy. Astron. Soc.* **405**, 503 (2010) [arXiv:0902.3232 [astro-ph.CO]];

- [14] C. Armendariz-Picon, JCAP **0407**, 007 (2004) [arXiv:astro-ph/0405267];  
 T. Koivisto and D. F. Mota, *Astrophys. J.* **679**, 1 (2008) [arXiv:0707.0279 [astro-ph]];  
 T. Koivisto and D. F. Mota, JCAP **0808**, 021 (2008) [arXiv:0805.4229 [astro-ph]];  
 G. Esposito-Farese, C. Pitrou and J. P. Uzan, *Phys. Rev. D* **81**, 063519 (2010) [arXiv:0912.0481 [gr-qc]].
- [15] M. Blomqvist, J. Enander and E. Mortsell, JCAP **1010**, 018 (2010) [arXiv:1006.4638 [astro-ph.CO]].
- [16] R. Kessler *et al.*, *Astrophys. J. Suppl.* **185**, 32 (2009) [arXiv:0908.4274 [astro-ph.CO]].
- [17] T. M. Davis *et al.*, *Astrophys. J.* **741**, 67 (2011) [arXiv:1012.2912 [astro-ph.CO]].
- [18] S. Gupta, T. D. Saini and T. Laskar, *Mon. Not. Roy. Astron. Soc.* **388**, 242 (2008) [arXiv:astro-ph/0701683];  
 S. Gupta and T. D. Saini, arXiv:1005.2868 [astro-ph.CO].
- [19] J. Colin, R. Mohayaee, S. Sarkar and A. Shafieloo, *Mon. Not. Roy. Astron. Soc.* **414**, 264 (2011) [arXiv:1011.6292 [astro-ph.CO]].
- [20] L. Campanelli, P. Cea, G. L. Fogli and A. Marrone, *Phys. Rev. D* **83**, 103503 (2011) [arXiv:1012.5596 [astro-ph.CO]].
- [21] D. J. Schwarz and B. Weinhorst, *Astron. Astrophys.* **474**, 717 (2007) [arXiv:0706.0165 [astro-ph]].
- [22] I. Antoniou and L. Perivolaropoulos, JCAP **1012**, 012 (2010) [arXiv:1007.4347 [astro-ph.CO]].
- [23] R. -G. Cai and Z. -L. Tuo, JCAP **1202**, 004 (2012) [arXiv:1109.0941 [astro-ph.CO]].
- [24] C. H. Lineweaver, L. Tenorio, G. F. Smoot, P. Keegstra, A. J. Banday and P. Lubin, *Astrophys. J.* **470**, 38 (1996) [arXiv:astro-ph/9601151].
- [25] D. Hutermeekers, R. Cabanac, H. Lamy and D. Sluse, *Astron. Astrophys.* **441**, 915 (2005) [arXiv:astro-ph/0507274];  
 D. Hutermeekers, A. Payez, R. Cabanac, H. Lamy, D. Sluse, B. Borguet and J. R. Cudell, arXiv:0809.3088 [astro-ph];  
 D. Hutermeekers and H. Lamy, arXiv:astro-ph/0012182.
- [26] R. Watkins, H. A. Feldman and M. J. Hudson, *Mon. Not. Roy. Astron. Soc.* **392**, 743 (2009) [arXiv:0809.4041 [astro-ph]].
- [27] B. Kalus, D. J. Schwarz, M. Seikel and A. Wiegand, arXiv:1212.3691 [astro-ph.CO].
- [28] M. Chevallier and D. Polarski, *Int. J. Mod. Phys. D* **10**, 213 (2001) [arXiv:gr-qc/0009008];

E. V. Linder, Phys. Rev. Lett. **90**, 091301 (2003) [arXiv:astro-ph/0208512].

[29] P. Duffett-Smith, ‘Practical Astronomy with your Calculator’ Cambridge University Press (1989).

[30] S. Nesseris and L. Perivolaropoulos, Phys. Rev. D **72**, 123519 (2005) [arXiv:astro-ph/0511040].

[31] A. Mariano and L. Perivolaropoulos, Phys. Rev. D **86** (2012) 083517 [arXiv:1206.4055 [astro-ph.CO]].

[32] M. Li, J. Pan, L. Gao, Y. Jing, X. Yang, X. Chi, L. Feng and X. Kang *et al.*, Astrophys. J. **761**, 151 (2012) [arXiv:1207.5338 [astro-ph.CO]].

[33] Jeffreys H., Theory of Probability, Oxford University Press, Oxford (1961).

[34] B. Rathaus, E. D. Kovetz and N. Itzhaki, arXiv:1301.7710 [astro-ph.CO].

[35] <http://www.mpe.mpg.de/jcg/grbgen.html>.

ID	z	$\mu \pm \sigma_\mu$	Equatorial Coordinate	ID	z	$\mu \pm \sigma_\mu$	Equatorial Coordinate
970228	0.70	$42.72 \pm 0.68$	$5^h 1^m 57^s, 11^\circ 46.4'$	030329	0.17	$39.73 \pm 0.29$	$10^h 44^m 50^s, 21^\circ 31'$
970508	0.84	$43.76 \pm 0.35$	$6^h 53^m 28^s, 79^\circ 17.4'$	030429	2.66	$46.61 \pm 0.53$	$12^h 13^m 18^s, -20^\circ 51.2'$
971214	3.42	$47.54 \pm 0.59$	$11^h 56^m 30^s, 65^\circ 12'$	030528	0.78	$44.31 \pm 0.54$	$17^h 4^m 2^s, -22^\circ 39'$
980613	1.10	$44.75 \pm 1.22$	$10^h 17^m 46^s, 71^\circ 29.9'$	040924	0.86	$43.61 \pm 0.55$	$2^h 6^m 19^s, 16^\circ 1'$
980703	0.97	$43.84 \pm 0.32$	$23^h 59^m 7^s, 8^\circ 35.6'$	041006	0.71	$43.92 \pm 0.42$	$0^h 54^m 53^s, 1^\circ 12'$
990123	1.61	$44.66 \pm 0.37$	$15^h 48^m 14^s, 51^\circ 31'$	050126	1.29	$45.74 \pm 0.52$	$18^h 32^m 27^s, 42^\circ 23'$
990506	1.31	$43.76 \pm 0.53$	$11^h 54^m 41^s, -26^\circ 45'$	050318	1.44	$45.95 \pm 0.44$	$3^h 18^m 43^s, -46^\circ 24.2'$
990510	1.62	$45.36 \pm 0.31$	$13^h 38^m 51^s, -80^\circ 32'$	050319	3.24	$47.73 \pm 0.93$	$10^h 16^m 38^s, 43^\circ 34'$
990705	0.84	$43.40 \pm 0.38$	$5^h 9^m 32^s, -72^\circ 9'$	050401	2.90	$45.94 \pm 0.55$	$16^h 31^m 31^s, 2^\circ 11'$
990712	0.43	$41.76 \pm 0.44$	$22^h 31^m 50^s, -73^\circ 24'$	050406	2.44	$48.03 \pm 0.70$	$2^h 17^m 43^s, -50^\circ 10'$
991208	0.71	$41.65 \pm 0.65$	$16^h 33^m 55^s, 46^\circ 26'$	050408	1.24	$45.09 \pm 0.72$	$12^h 1^m 55^s, 10^\circ 52'$
991216	1.02	$43.12 \pm 0.35$	$5^h 19^m 31^s, 11^\circ 11'$	050502	3.79	$47.24 \pm 0.64$	$13^h 29^m 46^s, 42^\circ 40'$
000131	4.50	$47.14 \pm 0.68$	$6^h 13^m 33^s, -51^\circ 55.6'$	050505	4.27	$48.49 \pm 0.59$	$9^h 27^m 8^s, 30^\circ 15'$
000210	0.85	$42.27 \pm 0.65$	$1^h 59^m 15^s, -40^\circ 40'$	050525	0.61	$43.28 \pm 0.37$	$18^h 32^m 35^s, 26^\circ 20'$
000911	1.06	$44.27 \pm 0.67$	$2^h 18^m 42^s, 7^\circ 48'$	050603	2.82	$44.66 \pm 0.58$	$2^h 39^m 55^s, -25^\circ 10.9'$
000926	2.07	$45.09 \pm 0.68$	$17^h 4^m 15^s, 51^\circ 46.6'$	050802	1.71	$45.52 \pm 0.98$	$14^h 37^m 9^s, 27^\circ 48'$
010222	1.48	$44.62 \pm 0.29$	$14^h 52^m 17^s, 43^\circ 2'$	050820	2.61	$46.27 \pm 0.59$	$22^h 29^m 36^s, 19^\circ 34.7'$
010921	0.45	$42.53 \pm 0.54$	$22^h 55^m 35^s, 40^\circ 56'$	050824	0.83	$44.07 \pm 1.19$	$0^h 48^m 57^s, 22^\circ 36'$
011211	2.14	$45.53 \pm 0.43$	$11^h 15^m 15^s, -21^\circ 56'$	050904	6.29	$49.27 \pm 0.47$	$0^h 54^m 41^s, 14^\circ 8.3'$
020124	3.20	$46.73 \pm 0.37$	$9^h 33^m 8^s, -11^\circ 35.6'$	050908	3.35	$47.00 \pm 0.76$	$1^h 21^m 51^s, -12^\circ 58'$
020405	0.70	$43.47 \pm 0.46$	$5^h 19^m 31^s, 11^\circ 11'$	050922	2.20	$45.57 \pm 0.52$	$21^h 9^m 34^s, -8^\circ 46.3'$
020813	1.25	$43.95 \pm 0.33$	$19^h 46^m 38^s, -19^\circ 35'$	051022	0.80	$43.77 \pm 0.28$	$23^h 56^m 0^s, 19^\circ 36'$
020903	0.25	$42.23 \pm 1.16$	$22^h 49^m 1^s, -20^\circ 56'$	051109	2.35	$45.84 \pm 0.80$	$22^h 1^m 11^s, 40^\circ 50.2'$
021004	2.32	$46.60 \pm 0.48$	$0^h 27^m 5^s, -19^\circ 6.1'$	051111	1.55	$44.54 \pm 0.60$	$23^h 12^m 38^s, 18^\circ 20'$
021211	1.01	$43.49 \pm 0.55$	$8^h 8^m 55^s, 6^\circ 44'$	060108	2.03	$48.85 \pm 1.07$	$9^h 47^m 58^s, 31^\circ 55'$
030115	2.50	$46.25 \pm 0.57$	$11^h 18^m 30^s, 15^\circ 2'$	060206	4.05	$46.37 \pm 0.60$	$13^h 31^m 47^s, 35^\circ 4.5'$
030226	1.98	$46.50 \pm 0.40$	$11^h 33^m 36^s, 25^\circ 49.9'$	060116	6.60	$48.33 \pm 0.92$	$5^h 38^m 48^s, -5^\circ 27'$
030323	3.37	$47.65 \pm 0.96$	$11^h 33^m 36^s, 25^\circ 49.9'$	060124	2.30	$46.78 \pm 0.38$	$5^h 8^m 10^s, 69^\circ 42.5'$
030328	1.52	$44.68 \pm 0.37$	$12^h 10^m 46^s, -9^\circ 22.5'$	060115	3.53	$47.78 \pm 0.79$	$3^h 36^m 11^s, 17^\circ 20.6'$

ID	z	$\mu \pm \sigma_\mu$	Equatorial Coordinate	ID	z	$\mu \pm \sigma_\mu$	Equatorial Coordinate
060210	3.91	$48.59 \pm 0.47$	$3^h 50^m 55^s, 27^\circ 2'$	060526	3.21	$47.17 \pm 0.41$	$15^h 31^m 23^s, 0^\circ 14.7'$
060223	4.41	$47.64 \pm 0.54$	$3^h 40^m 52^s, -17^\circ 8'$	060604	2.68	$46.23 \pm 0.57$	$22^h 28^m 58^s, -10^\circ 54'$
060418	1.49	$45.00 \pm 0.51$	$15^h 45^m 41^s, -3^\circ 38.6'$	060605	3.80	$47.04 \pm 0.68$	$21^h 28^m 35^s, -6^\circ 4'$
060502	1.51	$44.90 \pm 0.62$	$16^h 3^m 26^s, 66^\circ 36'$	060607	3.08	$46.24 \pm 0.55$	$21^h 58^m 51^s, -22^\circ 30.3'$
060510	4.90	$48.60 \pm 0.93$	$6^h 23^m 29^s, -1^\circ 10'$				

Table 6: Selected 67 GRB data points, added in positions described in the equatorial coordinates (right ascension and declination).